Numerical study of a channel flow with variable properties

By F. C. Nicoud

1. Motivation and objectives

In many industrial devices such as heat exchangers, piston engines, or propulsion systems strong temperature gradients arise in the near wall region even if the characteristic Mach number is close to zero. A strong coupling exists between momentum and energy equations caused by variations in the fluid properties, and the classical wall models for incompressible flows are not appropriate.

In the 1950's through the mid 1960's, many experimental studies focused on the assessment of global quantities at the wall (friction coefficient, Nusselt number) for laminar/turbulent flows with variable properties. Some empirical correlations of engineering interest were derived. More recent studies also deal with velocity and temperature profiles, and it has now reached the point that the supersonic compressible turbulent boundary layer with or without heat transfer is now well documented (see Bradshaw (1977), Fernholz & Finley (1980) and Spina *et al.* (1994) for reviews). The Strong Reynolds Analogy was introduced by Morkovin (1961) in the context of adiabatic boundary layers and has often been used in turbulence modeling. An extension was proposed by Gaviglio (1987) and subsequently Huang *et al.* (1995) for use in the presence of heat transfer. Some experimental data support these analogies in the case of a supersonic boundary layer over a cooled or heated wall and low speed flow on a slightly heated wall. Dimensional analysis of the inner layer shows that the law of the wall can be described in terms of two non-dimensional wall parameters, the friction Mach number $M_\tau = \frac{u_\tau}{c_w}$ and the heat flux parameter $B_q = \frac{q_w}{\rho_w C_p u_\tau T_w}$, where u_τ is the friction velocity $\sqrt{\frac{\tau_w}{\rho_w}}$, c_w the speed of sound, q_w the heat flux, C_p the constant-pressure specific heat, and T_w the temperature at the wall. Two cases, (M_τ,B_q)=(0.08,−0.05) and (0.12,−0.14), were considered in the DNS study of a supersonic channel flow performed by Coleman *et al.* (1995). These data were found in Huang & Coleman (1994) to support the validity of the Van Driest (1951) transformation

$$U^+_{VD} = \int_o^{u^+} \left(\frac{\rho}{\rho_w}\right)^{1/2} du^+ = \frac{1}{\kappa} ln y^+ + C$$

and suggest that the additive constant C is a function of both M_τ and B_q.

The case with large heat transfer and small Mach number has received very minor attention (W. Kays, private communication). The usefulness of the Van Driest transformation to retrieve the classical logarithmic law of the wall is not fully accepted in this case (Cheng & Ng (1982), Wardana *et al.* (1994), Wang & Pletcher (1996)) although some of the results in the latter reference appear to be erroneous

(P. Bradshaw, private communication). An LES of subsonic turbulent channel flow with constant heat flux performed by Dailey & Pletcher (1998) suggests that when the Mach number is close to 0 the constant C depends slightly on heat transfer. In the latter study, a Smagorinsky subgrid-scale model with Van-Driest damping at the wall was used to account for the subgrid scale effects. Since the value of C is expected to depend on conditions in the viscous and buffer layers (i.e. where the empirical Van Driest damping function is active), these LES data are questionable. In their experiments, Wardana *et al.* (1992, 1994) study the effect of strong wall heating on turbulence statistics of a channel flow. They provide high-order correlations for the velocity components and conclude that near the wall the ejection of low-speed fluid is intensified. They suppose that the local thermal expansion close to the heated wall is the driving force of the intensification. Since they do not use the Van Driest transformation to represent their mean velocity profiles, it is difficult to use their data to study the dependence of the additive constant on the heat transfer parameter B_q. Their experiments correspond to $B_q \approx$ 0, 0.073, 0.11, 0.13, and 0.17.

The objective of the present work is to study the case where the thermo-physical properties vary significantly in the absence of compressibility effects ($M = M_\tau = 0$). We perform a DNS of a *low speed* flow with a *large temperature gradient* in order to generate high-fidelity data which is not presently available. The configuration is a plane channel flow between two isothermal walls with temperatures T_1 and T_2 (see Fig. 1). Regarding the turbulence modeling, the objective is to provide more reliable information about the variation of the constant of integration C as a function of B_q. Other questions of interest relate to how good the Gaviglio's analogy is in the zero Mach number limit and the exact role of the fluid-property variations. A recent analytical study performed by Eames & Hunt (1997) shows how a lump of fluid experiences a lift force when it moves perpendicularly to a density gradient. A fundamental question that can be addressed using DNS is how this inviscid effect can modify the near wall streaks. Is it related to the intensification of the ejection events observed by Wardana *et al.* (1992, 1994)? The low Mach number approximation and the numerical method are discussed in Sections 2 and 3. The first DNS results are given in Section 4.

2. Low Mach number approximation

To avoid contamination of the solution by the non-physical acoustic modes reported in Coleman *et al.* (1995), a low Mach number approximation is first applied to the 3D compressible Navier-Stokes equations. In doing so, the density is decoupled from the pressure so that no acoustics are present in the computation. This also eliminates the acoustic CFL restriction on time step size.

To derive the low Mach number equations, one expands the dependent variables as a power series in $\epsilon = \gamma M^2$, which is a small parameter (see Paolucci (1982) for a complete discussion). Substituting these expansions into the Navier-Stokes equations and collecting the lowest order terms in ϵ yields:

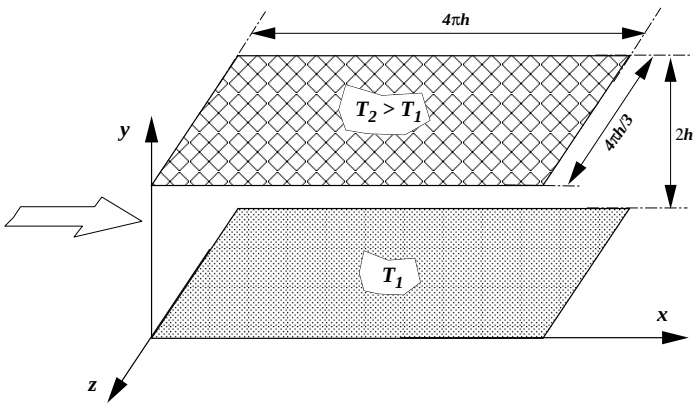

FIGURE 1. Computational domain.

$$\frac{\partial \rho}{\partial t} + \frac{\partial \rho u_j}{\partial x_j} = 0 \tag{1}$$

$$\rho \frac{\partial u_i}{\partial t} + \rho u_j \frac{\partial u_i}{\partial x_j} = -\frac{\partial P}{\partial x_i} + \frac{1}{R_e} \frac{\partial \tau_{ij}}{\partial x_j} \tag{2}$$

$$\rho C_p \frac{\partial T}{\partial t} + \rho C_p u_j \frac{\partial T}{\partial x_j} = \frac{1}{R_e P_r} \frac{\partial q_j}{\partial x_j} + \frac{\gamma - 1}{\gamma} \frac{dP_o}{dt} \tag{3}$$

In these equations, all the variables are normalized using the reference state ρ^{ref}, u^{ref}, $T^{\text{ref}} = P_o^{\text{ref}}/\rho^{\text{ref}}$, $C_p^{\text{ref}} = C_p^*(T^{\text{ref}})$, $\mu^{\text{ref}} = \mu^*(T^{\text{ref}})$, and $k^{\text{ref}} = k^*(T^{\text{ref}})$ where the superscript * represent dimensional quantities. Also $R_e = \rho^{\text{ref}} u^{\text{ref}} L^{\text{ref}}/\mu^{\text{ref}}$ and $P_r = \mu^{\text{ref}} C_p^{\text{ref}}/k^{\text{ref}}$ are the Reynolds and the Prandtl number while γ is the ratio of specific heats at the reference state. u_i, ρ, T, and C_p stand for the non-dimensionalized velocity vector, density, temperature, and specific heat. $\tau_{ij} = \mu \left(\frac{\partial u_i}{\partial x_j} + \frac{\partial u_j}{\partial x_i} - \frac{2}{3} \delta_{ij} \frac{\partial u_k}{\partial x_k} \right)$ and $q_j = k \frac{\partial T}{\partial x_j}$ are the viscous stress tensor and the heat flux vector respectively. Moreover, P may be interpreted as the hydrodynamic pressure. In the low-Mach number approximation, the thermodynamic pressure P_o only depends on time and must be computed if it is not constant. The equation of state is simply:

$$P_o = \rho T \tag{4}$$

Since density is uniquely determined by the temperature (and the thermodynamic pressure which is constant in space), the energy equation acts as a constraint which is enforced by the hydrodynamic pressure. This constraint is:

$$\frac{\partial u_i}{\partial x_i} = \frac{1}{P_o(t) C_p} \left[\frac{1}{R_e P_r} \frac{\partial}{\partial x_j} \left(k \frac{\partial T}{\partial x_j} \right) + \left(\frac{\gamma - 1}{\gamma} - C_p \right) \frac{dP_o}{dt} \right]$$

Integrating over the flow domain V leads to the following ODE for the thermodynamic pressure in a closed system:

$$\frac{dP_o}{dt} = \frac{1}{\int_V \left(\frac{\gamma - 1}{\gamma} - C_p \right) dV} \left[\frac{1}{R_e P_r} \int_V \frac{\partial}{\partial x_j} \left(k \frac{\partial T}{\partial x_j} \right) dV + P_o(t) \int_V u_i \frac{\partial C_p}{\partial x_i} dV \right] \tag{5}$$

Since $\int_V \frac{\partial}{\partial x_j}\left(k\frac{\partial T}{\partial x_j}\right)dV = \int_S k\frac{\partial T}{\partial x_j}dS_j$, this relation expresses how the rate of change of the mean pressure is affected by the heat flux through the surface S of the domain V and the gradients of heat capacity of the gas. In many practical applications the fluid may be considered as a calorifically perfect gas so that $C_P = 1$ and the time derivative of P_o is simply:

$$\frac{dP_o}{dt} = \frac{\gamma}{V}\frac{1}{R_e P_r}\int_V \frac{\partial}{\partial x_j}\left(k\frac{\partial T}{\partial x_j}\right)dV = \frac{1}{V}\frac{1}{R_e P_r}\int_S k\frac{\partial T}{\partial x_j}dS_j \tag{6}$$

Thus the constraint on the velocity field becomes:

$$\frac{\partial u_i}{\partial x_i} = \frac{1}{P_o(t) R_e P_r}\left[\frac{\partial}{\partial x_j}\left(k\frac{\partial T}{\partial x_j}\right) - \frac{1}{V}\int_V \frac{\partial}{\partial x_j}\left(k\frac{\partial T}{\partial x_j}\right)dV\right] \tag{7}$$

If the system considered is open, then the thermodynamic pressure is set by atmospheric conditions. If it is closed, then the amount of mass in it, M_0, is constant over time so that by integrating the equation of state over the whole domain one obtains the following expression for the thermodynamic pressure:

$$P_o(t) = \frac{M_0}{\int_V \frac{1}{T}dV} \tag{8}$$

Note that, in the limit of an inviscid flow of a calorifically perfect gas, the thermodynamic pressure remains constant over time (from Eq. (6)) and the velocity field is divergence-free (from Eq. (7)). The solution (ρ, u_i, T, P, P_o) is completely described by Eqs. (1)-(5). The constraint (7) should also be satisfied since it is a linear combination of Eqs. (1), (3), and (4).

3. Numerical method

The numerical method chosen for solving the variable density momentum and temperature equations is a generalization of a fully conservative fourth order spatial scheme developed for incompressible flows on staggered grids by Morinishi *et al.* (1998). A scheme to solve the momentum equations in non-conservative form is described in the following subsection. After that, a scheme with 'good' conservative properties is discussed.

3.1 Scheme in non-conservative form

For a uniform mesh, the advective term in the momentum equation (2) is discretized as:

$$\begin{aligned}\rho u_j \frac{\partial u_i}{\partial x_j} \quad \equiv \quad & \overline{\frac{9}{8}\left(\frac{9}{8}\overline{\rho^{(4j)}u_j}^{1x_i} - \frac{1}{8}\overline{\rho^{(4j)}u_j}^{3x_i}\right)\frac{\delta_1 u_i}{\delta_1 x_j}}^{1x_j} \\ & \overline{-\frac{1}{8}\left(\frac{9}{8}\overline{\rho^{(4j)}u_j}^{1x_i} - \frac{1}{8}\overline{\rho^{(4j)}u_j}^{3x_i}\right)\frac{\delta_3 u_i}{\delta_3 x_j}}^{3x_j}\end{aligned} \tag{9}$$

where the finite-difference operator with stencil n acting on ϕ with respect to x_i is defined as

$$\frac{\delta_n \phi}{\delta_n x_i} = \frac{\phi(x_i + nh_i/2) - \phi(x_i - nh_i/2)}{nh_i}$$

and the interpolation operator with stencil n acting on ϕ in the x_i direction is

$$\overline{\phi}^{nx_i} = \frac{\phi(x_i + nh_i/2) + \phi(x_i - nh_i/2)}{2}.$$

$\rho^{(4j)} = \frac{9}{8}\overline{\rho}^{1x_j} - \frac{1}{8}\overline{\rho}^{3x_j}$ is a fourth order interpolation of ρ in the x_j direction. When the density is constant, Eq. (9) reduces to the advective form (Adv.-S4) in Morinishi *et al.* (1998). The pressure term in Eq. (2) in discretized by:

$$\frac{\partial P}{\partial x_i} \equiv (Pres.)_i = (\nabla_d P)_i = \frac{9}{8}\frac{\delta_1 P}{\delta_1 x_i} - \frac{1}{8}\frac{\delta_3 P}{\delta_3 x_i} \tag{10}$$

and the discrete divergence operator is defined consistently: $\frac{\partial u_i}{\partial x_i} \equiv \nabla_d \cdot (u_i) = \frac{9}{8}\frac{\delta_1 u_i}{\delta_1 x_i} - \frac{1}{8}\frac{\delta_3 u_i}{\delta_3 x_i}$. The viscous terms in Eq. (2) are written using the generic form:

$$\begin{aligned} \frac{\partial}{\partial x_j}\left(\mu \frac{\partial u_i}{\partial x_j}\right) \quad \equiv \quad & \frac{9}{8}\frac{\delta_1}{\delta_1 x_j}\left[\mu^{(4i),(4j)}\left(\frac{9}{8}\frac{\delta_1 u_i}{\delta_1 x_j} - \frac{1}{8}\frac{\delta_3 u_i}{\delta_3 x_j}\right)\right] \\ & -\frac{1}{8}\frac{\delta_3}{\delta_3 x_j}\left[\mu^{(4i),(4j)}\left(\frac{9}{8}\frac{\delta_1 u_i}{\delta_1 x_j} - \frac{1}{8}\frac{\delta_3 u_i}{\delta_3 x_j}\right)\right] \end{aligned} \tag{11}$$

The advective term for the temperature is discretized as:

$$\rho u_j \frac{\partial T}{\partial x_j} \equiv \frac{9}{8}\overline{\rho^{(4j)} u_j \frac{\delta_1 T}{\delta_1 x_j}}^{1x_j} - \frac{1}{8}\overline{\rho^{(4j)} u_j \frac{\delta_3 T}{\delta_3 x_j}}^{3x_j} \tag{12}$$

A semi-implicit time marching algorithm is used in which the diffusion terms in the wall normal direction are treated implicitly with a Crank-Nicolson scheme while a third order Runge-Kutta scheme is used for all other terms. The temperature equation is advanced first so that ρ^{n+1} is known via the state equation $\rho = P_o/T$, where P_o is first assessed using Eq. (8) written at time $n+1$. Then a fractional step method is used to solve the momentum equation.

$$\begin{aligned} \rho^{(4i),n+1}\frac{u_i^{n+1} - u_i^n}{\Delta t} &= \rho^{(4i),n+1}\frac{u_i^{n+1} - \hat{u}_i}{\Delta t} + \rho^{(4i),n+1}\frac{\hat{u}_i - u_i^n}{\Delta t} \\ &= \frac{\beta_k}{2}\left(I^{n+1} + I^n\right) + \gamma_k E^n + \zeta_k E^{n-1} - 2\beta_k \nabla_d P^n - 2\beta_k \nabla_d \delta P^{n+1} \end{aligned} \tag{13}$$

where I and E represent all the spatial implicit and explicit terms except for the pressure at n and the pressure update $\delta P^{n+1} = P^{n+1} - P^n$. The parameters β_k, γ_k, and ζ_k $(k = 1, 3)$ are chosen so that the mixed Runge-Kutta/Crank-Nicolson time stepping is recovered after the third substep (Spalart, 1987). Equation (13)

is then split into a decoupled set which is a second-order approximation in time to the original equation:

$$\rho^{(4i),n+1}\frac{\hat{u}_i - u_i^n}{\Delta t} = \frac{\beta_k}{2}\left(I^{n+1} + I^n\right) + \gamma_k E^n + \zeta_k E^{n-1} - 2\beta_k \nabla_d P^n \tag{14}$$

$$\rho^{(4i),n+1}\frac{u_i^{n+1} - \hat{u}_i}{\Delta t} = -2\beta_k \nabla_d \delta P^{n+1} \tag{15}$$

Equation (14) is solved for $\hat{u}_i$ by using the discretizations (9), (10), and (11). Then (15) is divided by $\rho^{(4i),n+1}$ before its discrete divergence is taken to obtain:

$$\nabla_d \cdot \left(\frac{1}{\rho^{(4i),n+1}}\nabla_d \delta P\right) = \frac{1}{2\beta_k \Delta t}\left(\nabla_d \cdot \hat{u}_i - \nabla_d \cdot u_i^{n+1}\right) = S \tag{16}$$

A similar Poisson equation with variable coefficients was solved in Bell & Marcus (1992) to impose the divergence-free constraint for variable-density flows.

Since the transport equation for T has been advanced prior to the momentum equation, the last term in the equation for the pressure variation is known from Eq. (7), written at time $n+1$. The non-linear Poisson equation (16) for the pressure is solved using the iterative procedure:

$$\nabla_d \cdot \left(\frac{1}{\left\langle \rho^{(4i),n+1}\right\rangle}\nabla_d \delta P^{k+1}\right) = \frac{1}{2\beta_k \Delta t}\left(S + \nabla_d \cdot \left(\left[\frac{1}{\left\langle \rho^{(4i),n+1}\right\rangle} - \frac{1}{\rho^{(4i),n+1}}\right]\nabla_d \delta P^k\right)\right) \tag{17}$$

where $<>$ denote a plane averaging in the two homogeneous directions x and z. Each sub-iteration is solved exactly using a Fast Poisson Solver. The advantage of solving Eq. (16) to update the pressure is that the divergence-free constraint is recovered in the inviscid limit, as it has to be from Eq. (7). This is not the case when a backward approximation of $\frac{\partial \rho}{\partial t}$ is used to compute the source term of a linear Poisson equation for δP as proposed by McMurthry *et al.* (1986), Cook & Riley (1996). The other advantage is that the pressure terms remain energy conserving in the inviscid limit as discussed in the following subsection. Several basic test cases have been computed to validate the above procedure (see Subsection 3.3).

3.2 Toward a fully conservative scheme

Although the previous scheme was found to be accurate, it only conserves momentum and kinetic energy to its own order of accuracy. Experience has shown that the latter quantity must be conserved exactly if a robust and dissipation-free numerical method is sought. Morinishi *et al.* (1998) developed a set of fully conservative (mass, momentum, and kinetic energy) high order schemes for incompressible flow. In the general case of the Navier-Stokes equations without body force, the transport equation for the kinetic energy per unit volume ρk reads:

$$\frac{\partial \rho k}{\partial t} + \frac{\partial \rho u_j k}{\partial x_j} = P S_{jj} - \frac{\partial P u_j}{\partial x_j} + \frac{\partial \tau_{ij} u_i}{\partial x_j} - \tau_{ij} S_{ij} \tag{18}$$

Let us consider a periodic (or infinite) domain so that, after Eq. (18) is integrated over the domain, the flux terms $\frac{\partial \rho u_j k}{\partial x_j}$ and $\frac{\partial P u_j}{\partial x_j}$ make no contribution. Due to the dissipation term $\tau_{ij} S_{ij}$, the question of conservation of the kinetic energy is only relevant in the inviscid limit where $\tau_{ij} = 0$. We know from Eq. (7) that in this limit the velocity field is divergence-free, that is $S_{jj} = 0$. Thus global conservation of kinetic energy is a common feature of incompressible and low Mach number flows. The purpose of this section is to investigate how this property can be extended in discrete space. Let us define the following discrete approximations of the possible forms for the non-linear term in the momentum equation:

$$\begin{aligned}(Adv.)_i &= \overline{\tfrac{9}{8}\left(\tfrac{9}{8}\overline{\rho^{(4j)}u_j}^{1x_i} - \tfrac{1}{8}\overline{\rho^{(4j)}u_j}^{3x_i}\right)\tfrac{\delta_1 u_i}{\delta_1 x_j}}^{1x_j} \\ &\quad \overline{-\tfrac{1}{8}\left(\tfrac{9}{8}\overline{\rho^{(4j)}u_j}^{1x_i} - \tfrac{1}{8}\overline{\rho^{(4j)}u_j}^{3x_i}\right)\tfrac{\delta_3 u_i}{\delta_3 x_j}}^{3x_j}\end{aligned} \tag{19}$$

$$\begin{aligned}(Div.)_i &= \tfrac{9}{8}\tfrac{\delta_1}{\delta_1 x_j}\left[\left(\tfrac{9}{8}\overline{\rho^{(4j)}u_j}^{1x_i} - \tfrac{1}{8}\overline{\rho^{(4j)}u_j}^{3x_i}\right)\overline{u_i}^{1x_j}\right] \\ &- \tfrac{1}{8}\tfrac{\delta_3}{\delta_3 x_j}\left[\left(\tfrac{9}{8}\overline{\rho^{(4j)}u_j}^{1x_i} - \tfrac{1}{8}\overline{\rho^{(4j)}u_j}^{3x_i}\right)\overline{u_i}^{3x_j}\right]\end{aligned} \tag{20}$$

$$(Skew.)_i = \frac{1}{2}\left((Adv.)_i + (Div.)_i\right) \tag{21}$$

The forms $(Adv.)$, $(Div.)$, and $(Skew.)$ are the discrete equivalent to the advective $\rho u_j \frac{\partial u_i}{\partial x_j}$, conservative $\frac{\partial \rho u_i u_j}{\partial x_j}$, and skew-symmetric $\frac{1}{2}\left(\rho u_j \frac{\partial u_i}{\partial x_j} + \frac{\partial \rho u_i u_j}{\partial x_j}\right)$ form of the convective term. The following relations hold between these three discrete forms:

$$(Div.)_i = (Adv.)_i + u_i\left(\frac{9}{8}\overline{(Cont.)}^{1x_i} - \frac{1}{8}\overline{(Cont.)}^{3x_i}\right) \tag{22}$$

$$(Skew.)_i = (Adv.)_i + \frac{1}{2}u_i\left(\frac{9}{8}\overline{(Cont.)}^{1x_i} - \frac{1}{8}\overline{(Cont.)}^{3x_i}\right) \tag{23}$$

$$(Skew.)_i = (Div.)_i - \frac{1}{2}u_i\left(\frac{9}{8}\overline{(Cont.)}^{1x_i} - \frac{1}{8}\overline{(Cont.)}^{3x_i}\right) \tag{24}$$

where $(Cont.) = \frac{9}{8}\frac{\delta_1 \rho^{(4j)} u_j}{\delta_1 x_j} - \frac{1}{8}\frac{\delta_3 \rho^{(4j)} u_j}{\delta_3 x_j}$ is the discrete form of the divergence of ρu_j.

A key assumption in the semi-discrete analysis proposed in Morinishi *et al.* (1998) for incompressible flow is that the operator $(Cont.)$ is identically zero so that the three forms $(Div.)_i$, $(Adv.)_i$, and $(Skew.)_i$ are equivalent. Since $(Div.)_i$ is conservative *a priori* for the momentum equation and $(Skew.)_i$ is conservative *a priori* in the kinetic energy equation, a fully conservative scheme is obtained as soon as the velocity constraint $\frac{\partial u_j}{\partial x_j} = 0$ is imposed properly through the pressure correction step. In the present case where the density is not constant, the velocity constraint $\frac{\partial u_j}{\partial x_j} = 0$ (in the inviscid limit) does not imply that $\frac{\partial \rho u_j}{\partial x_j}$ is zero. Thus the discrete operators $(Div.)_i$, $(Adv.)_i$, and $(Skew.)_i$ are not equivalent in the low Mach number case, meaning that a fully discrete analysis (including the time discretization) must be conducted to achieve conservation of kinetic energy.

A conservative scheme for the momentum can be derived by solving the divergence form of Eq. (2). The first guess for the velocity is obtained by:

$$\frac{\hat{\rho}^{(4i)}\hat{u}_i - \rho^{(4i),n}u_i^n}{\Delta t} = -\gamma_k(Div.)_i^n - \zeta_k(Div.)_i^{n-1} - 2\beta_k(Pres.)_i^n \tag{25}$$

where $\hat{\rho}$ can be either any intermediate value. Then the projection step is:

$$u_i^{n+1} = \frac{\hat{\rho}^{(4i)}}{\rho^{(4i),n+1}}\hat{u}_i - 2\beta_k\frac{1}{\rho^{(4i),n+1}}\nabla_d\delta P\Delta t \tag{26}$$

where the Poisson equation for δP must be:

$$\nabla_d\cdot\left(\frac{1}{\rho^{(4i),n+1}}\nabla_d\delta P\right) = \frac{1}{2\beta_k\Delta t}\left(\nabla_d\cdot\left(\frac{\hat{\rho}^{(4i)}}{\rho^{(4i),n+1}}\hat{u}_i\right) - \nabla_d\cdot u_i^{n+1}\right) \tag{27}$$

Obviously, Eqs. (25), (26), and (27) constitute a scheme which is momentum conserving. To investigate whether it also conserves kinetic energy, let us multiply Eq. (25) by $\hat{u}_i + u_i^n$ and integrate over the whole domain. The overall contribution of the first pressure term in the kinetic energy equation reads as:

$$\int_V u_i^n(Pres.)_i^n dV = \int_V\left(\frac{9}{8}\overline{u_i^n\frac{\delta_1 P}{\delta_1 x_i}}^{1x_i} - \frac{1}{8}\overline{u_i^n\frac{\delta_3 P}{\delta_3 x_i}}^{3x_i}\right)dV \tag{28}$$

where

$$\frac{9}{8}\overline{u_i^n\frac{\delta_1 P}{\delta_1 x_i}}^{1x_i} - \frac{1}{8}\overline{u_i^n\frac{\delta_3 P}{\delta_3 x_i}}^{3x_i} = \frac{9}{8}\frac{\delta_1 u_i^n\overline{P}^{1x_i}}{\delta_1 x_i} - \frac{1}{8}\frac{\delta_3 u_i^n\overline{P}^{3x_i}}{\delta_3 x_i} - P\left(\frac{9}{8}\frac{\delta_1 u_i^n}{\delta_1 x_i} - \frac{1}{8}\frac{\delta_3 u_i^n}{\delta_3 x_i}\right) \tag{29}$$

The first two terms do not contribute because they are in divergence form; the last two are identically zero because the non-linear Poisson equation (27) is solved with $\nabla_d\cdot u_i^{n+1} = \frac{9}{8}\frac{\delta_1 u_i^n}{\delta_1 x_i} - \frac{1}{8}\frac{\delta_3 u_i^n}{\delta_3 x_i} = 0$ imposed in the source term. The contribution of the term $\hat{u}_i(Pres.)_i^n$ is of order Δt because $\hat{u}_i = u_i^n + O(\Delta t)$. Using Eq. (24), the overall contribution of the RHS of Eq. (25) may be written as

$$\begin{array}{rc} & \int_V(\hat{u}_i+u_i^n)\left(-\gamma_k(Skew.)_i^n - \zeta_k(Skew.)_i^{n-1}\right)dV \\ - & \gamma_k\int_V\frac{\hat{u}_i+u_i^n}{2}u_i^n\left(\frac{9}{8}\overline{(Cont.)^n}^{1x_i} - \frac{1}{8}\overline{(Cont.)^n}^{3x_i}\right)dV \\ - & \zeta_k\int_V\frac{\hat{u}_i+u_i^n}{2}u_i^{n-1}\left(\frac{9}{8}\overline{(Cont.)^{n-1}}^{1x_i} - \frac{1}{8}\overline{(Cont.)^{n-1}}^{3x_i}\right)dV \\ + & O(\Delta t)\end{array} \tag{30}$$

The first integral in (30) contributes to the order Δt because $(Skew.)_i$ is kinetic energy conserving in nature and because $\hat{u}_i$, u_i^n, and u_i^{n-1} are equal to the order Δt. On the other hand, the contribution of the LHS of (25) may be written:

$$\int_V\frac{\hat{\rho}^{(4i)}\left(\hat{u}_i\right)^2 - \rho^{(4i),n}\left(u_i^n\right)^2}{\Delta t}dV + \int_V u_i^n\hat{u}_i\frac{\hat{\rho}^{(4i)} - \rho^{(4i),n}}{\Delta t}dV \tag{31}$$

Comparing Eqs. (30) and (31) it appears that the discrete rate of change of the kinetic energy (the first integral in Eq. (31)) is at most of order Δt if one defines the intermediate density as:

$$\frac{\hat{\rho}-\rho^n}{\Delta t} = -\gamma_k (Cont.)^n - \zeta_k (Cont.)^{n-1} \tag{32}$$

In the context of second order scheme, the same definition of $\hat{\rho}$ was adopted (C. Pierce, private communication) to achieve approximate conservation of kinetic energy. Multiplying the projection step Eq. (26) by $\hat{u}_i + u_i^{n+1}$ and integrating over the whole domain, the following expression can be derived:

$$\int_V \frac{\rho^{(4i),n+1}\left(u_i^{n+1}\right)^2 - \hat{\rho}^{(4i)}\left(\hat{u}_i\right)^2}{\Delta t} dV = \int_V \hat{u}_i u_i^{n+1} \frac{\hat{\rho}^{(4i)} - \rho^{(4i),n+1}}{\Delta t} dV + O(\Delta t) \tag{33}$$

This shows that the global rate of change of the kinetic energy is of order Δt only if $\hat{\rho}^{(4i)} - \rho^{(4i),n+1} = O(\Delta t^n)$, $n \geq 2$. Unfortunately, n is only 1 in the most general case. A conservative scheme is obtained if one accepts that the state equation (4) is verified to the order Δt only, viz:

$$\rho^{n+1} = \hat{\rho} = \frac{P_o}{T^{n+1}} + O(\Delta t) \tag{34}$$

In this case, the error in the kinetic energy conservation is at most of order Δt.

3.3 Basic test cases

The following test cases were designed to check the accuracy of the numerical method. In what follows, AdvSC and DivSC stand for the schemes discussed in Sections 3.1 and 3.2 respectively. Except as otherwise stated (Section 3.3.2), the state equation (4) is enforced exactly.

3.3.1 1D Euler convection

If the Peclet number is infinite, the velocity field must be divergence-free; that is, u must be constant in 1D. Also, the pressure should remain constant. To test the ability of the two formulations to reproduce this feature of Eqs. (1)-(3), consider the domain $0 \leq x \leq 1$, periodic in x. The initial condition is $u = u_0 = 1$, $P = 0$, and $T = 1 + A \exp\left[-\left(\frac{x-x_0}{a}\right)^2\right]$ with $A = 1$, $x_0 = 0.5$, and $a = 0.05$. When the grid contains $N_x = 24$ points, only 6 points are used to describe a Gaussian perturbation. Figure 2 shows $P_{\rm rms}/\rho_0 u_0^2$ as a function of the grid spacing, where three grid levels were considered: 24, 48, and 96 points in x. The rms of pressure is assessed for the time $t = 20a/u_0$. The CFL number is of order 0.5 in all cases. Both schemes are fourth-order accurate in space, but AdvSC is exact for this particular test case. The divergence is zero in both cases because it is explicitly enforced through the Poisson equations (27) for DivSC and (16) for AdvSC.

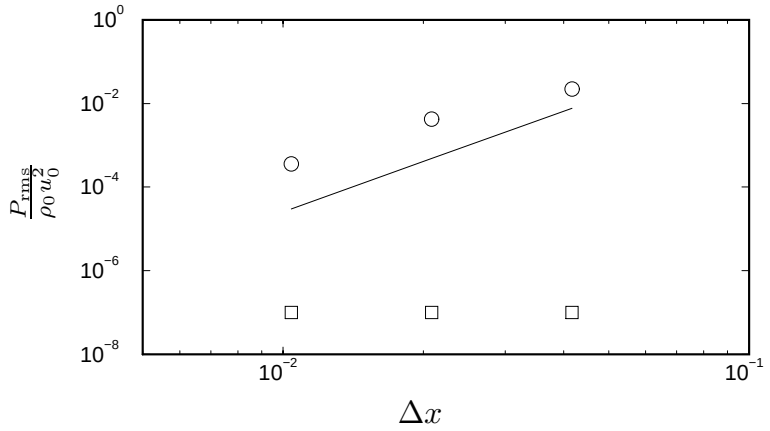

FIGURE 2. Root-mean-square of pressure as a function of the grid spacing at time $t = 20a/u_0$. ——— : $P_{\rm rms} \propto \Delta x^4$; ∘ : DivSC; □ : AdvSC.

3.3.2 Small 1D perturbations

In the case where the Reynolds number is finite but where the perturbation in temperature is small ($A << 1$), the analytical resolution of Eqs. (1)-(3) can be conducted and the structure of the perturbation which propagates is given by:

$$\rho' = -\frac{\rho_0}{T_0} T' \tag{35}$$

$$u' = \frac{1}{R_e P_r} \frac{\partial T'}{\partial x} \tag{36}$$

$$p' = \frac{4}{3 R_e^2 P_r^2} \frac{\partial^2 T'}{\partial x^2} \left(P_r - \frac{3}{4} \right) \tag{37}$$

An interesting feature is that the pressure fluctuation should vanish in the limit $P_r = \frac{3}{4}$. Figure 3 shows the error in Eq. (37) in the case $N_x = 24$, $a = 0.05$, $A = 0.01$, and $R_e = 50$. The initial condition is uniform for u and P and the physical time simulated is large enough ($t \approx 160a/u_0$) so that the values reported in the figure are asymptotic values. For this poor resolution, the remaining error for DivSC is much greater than for AdvSC.

3.3.3 2D Random perturbations

To validate the results of Section 3.2 with numerical tests, inviscid flow simulations were performed on a 2D periodic domain. The analytical solution dictates that the total momentum in each direction $\langle \rho u_i \rangle$ and total kinetic energy $\langle K \rangle = \frac{1}{2} \langle \rho u_i^2 \rangle$ should be conserved in time. The domain is $0 \leq x \leq L$, $0 \leq y \leq L$, and a 24x24 mesh is used. Solenoidal velocity fields are used as the initial condition together with random temperature fluctuations. The initial mean kinetic energy is of order 1.5 while $T_{\rm rms} \approx 0.15 < T >$ at $t = 0$. Figure 4 shows the relative error for the total kinetic energy $\frac{\langle K_0 - K \rangle}{\langle K_0 \rangle}$ after an integration time of $t = 0.125 L / \sqrt{\langle K_0 \rangle}$. As expected from Section 3.2, the error for the scheme DivSC is not a function of the time step only, but also of space the space discretization. On the other hand, it appears that

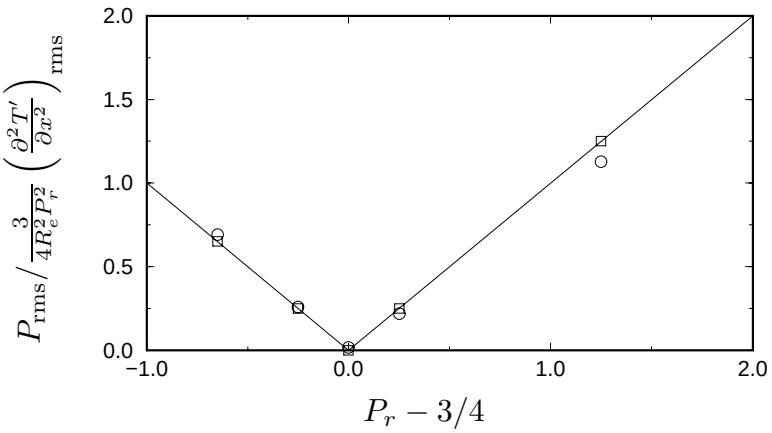

FIGURE 3. Root-mean-square of pressure as a function of the Prandtl number. $P_{\rm rms}$ is non-dimensionalized by its theoretical value as a function of T'. ——— : exact solution Eq. (37); ○ : DivSC; □ : AdvSC.

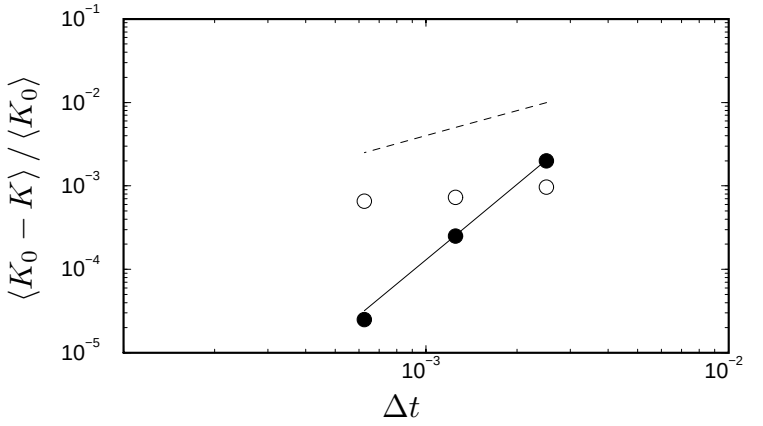

FIGURE 4. Kinetic energy conservation error as a function of the time step. ——— : Δt^3 behavior; – – – – : Δt behavior; ○ : DivSC; ● : DivSC with approximate equation of state, Eq. (34).

the same scheme with the approximate equation of state, Eq. (34), produces no violation in the conservation of kinetic energy due to the spatial scheme. The measured error behaves like Δt^3 instead of Δt as predicted in 3.2 . Indeed, a single substep of the time integration was considered in the analysis so that the cancellation of error in the full third-order Runge-Kutta procedure was not accounted for.

3.3.4 Linear stability in a channel

To check the accuracy of the code in the case where the physical properties vary in space and time through the temperature, the evolution of low amplitude eigenmodes in laminar channel flow is simulated. The linear stability problem in a channel flow between two isothermal walls with temperature $T_1 = 1 - \frac{\delta T}{2}$ and $T_2 = 1 + \frac{\delta T}{2}$ was studied by Suslov & Paolucci (1995) under the low Mach number assumption. They found that the critical Reynolds number increases with the parameter $\frac{\delta T}{2}$. It

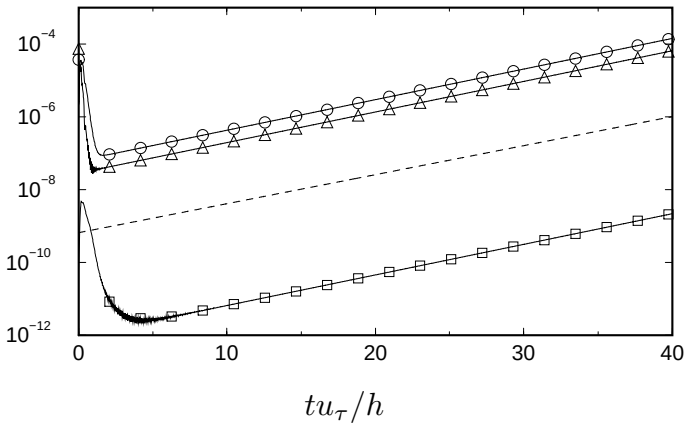

FIGURE 5. Time evolution of the global energy of the fluctuations in the computational domain. ---- : linear stability theory (Suslov & Paolucci (1995)); —○— : $< u'^2 >$; —△— : $< v'^2 >$; —□— : $< T'^2 >$.

is of order 40000 for $\frac{\delta T}{2} = 0.4$, compared to 5772 in the isothermal case ($\delta T = 0$). In their analysis the dimensionless thermal conductivity and dynamic viscosity are given by Sutherland's law:

$$k(T) = T^{3/2}\frac{1+S_k}{T+S_k} \qquad\qquad \mu(T) = T^{3/2}\frac{1+S_\mu}{T+S_\mu} \tag{38}$$

where $S_k = 0.648$ and $S_\mu = 0.368$ for air at $T_{\rm ref} = 300K$ and normal pressure. The molecular Prandtl number is 0.76. In the computation, the length of the periodic domain in x is $L = 2\pi/\alpha$, where α is the wave number of the mode of interest. The initial condition consists of a small amplitude (0.01%) random noise on u, v superimposed to the laminar solution of the problem (Suslov & Paolucci (1995)). A stretched grid is used in the normal direction in order to capture the eigenvector accurately near the walls. The wall normal velocity points are distributed according to a hyperbolic tangent function ($j = 0, 1, 2, ..., N$):

$$y_v(j) = y_{j+\frac{1}{2}} = \frac{\tanh(\gamma\left(\frac{2j}{N}-1\right))}{\tanh(\gamma)} \tag{39}$$

A typical result is shown in Fig. 5. In this case the resolution is 24x100 with $\gamma = 2$ for the stretching parameter. The CFL number is fixed at 1. The length of the domain is $L = 2.4\pi h$ ($\alpha = \frac{5}{6}\frac{1}{h}$) and the Reynolds number is 45000, based on the maximum velocity and the channel half-height h. The temperature ratio is $\frac{T_2}{T_1} = 2.33$, i.e. $\frac{\delta T}{2} = 0.4$. For these conditions, the flow is linearly unstable (see Suslov & Paolucci (1995)). The code predicts a reasonable growth rate for this eigenmode. Note that a fairly long time ($10h/u_\tau$) is needed for the mode to settle in. Once the transition phase is finished, the temperature and the two velocity components develop with exactly the same rate, as dictated by the linear stability theory. DivSC and AdvSC give similar results (AdvSC shown).

4. Results

Two DNS's of a channel flow are performed to study the effect of the temperature gradient on the flow. Details of the test cases adopted are given in Table I.

Case	T_2/T_1	$R_{\tau 1}$	$R_{\tau 2}$	R_{ec}	Δx^+	Δy^+	Δz^+
A	1.01	180	180	3300	18.8	$0.25-10$	6.28
B	2	200	82	2700	$8.4-21.5$	$0.25-9$	$2.8-7.2$

Table I: Numerical parameters of the two computations performed.

In each case the domain size is ($4\pi h$,$2h$,$4\pi/3h$) and the grid contains 120x100x120 cells. The statistics shown for Case B were obtained over a time period of order $5.7h/\overline{u_\tau}$, where $\overline{u_\tau} = \frac{u_{\tau 1}+u_{\tau 2}}{2}$ is the mean friction velocity. The wall normal velocity points are distributed according to Eq. (39) with $\gamma = 2.5$ for Case A. For Case B, the Reynolds number near the hot wall is expected to be smaller than near the cold wall and the following non-symmetric distribution is used:

$$y_v(j) = 2\frac{\hat{y}_v(j)+1}{\hat{y}_v(N)+1} - 1 \tag{40}$$

with

$$\hat{y}_v(j) = \frac{\tanh(\gamma\left(\frac{2\alpha j}{N}-1\right))}{\tanh(\gamma)} \tag{41}$$

and $\gamma = 2.5$ and $\alpha = 0.9$. Buoyancy effects are neglected and the dimensionless thermal conductivity and dynamic viscosity are given by Sutherland's law (see Section 3.3.4). The molecular Prandtl number is 0.76. In Case A the temperature is almost uniform and the results may be compared to previous incompressible DNS performed by Kim & Moin (1987) and Kasagi (1992) as well as semi-empirical correlations derived by Kader (1981) for the passive scalar case. In Case B one expects the temperature (density) variations to be large enough to modify the momentum balance through both viscous and inviscid effects. The analytical work of Eames & Hunt (1997) shows that when a body moves perpendicularly to a density gradient, a lift force, $C_L(U \times \nabla\rho) \times U$, pushes it towards the denser fluid. Thus the order of magnitude of the inviscid lift acting on a turbulent structure in the channel flow is $C_L u_\tau^2 \Delta\rho/h$. Requiring that this inviscid force is of the same order of magnitude as the viscous force, $\tau_w/h = \rho u_\tau^2/h$, one obtains the estimate $\Delta\rho/\rho \simeq 1/C_L$, where C_L is the lift coefficient. With C_L in the range $1/4-1/2$, the inviscid lift related to the density gradient may balance the viscous forces for $\Delta\rho/\rho$ in the range $2-4$. Note that one overestimates the required $\Delta\rho/\rho$ by assuming that the density gradient in the near wall region is equal to the mean density gradient $\Delta\rho/h$. Case B corresponds to $T_2/T_1 = 2$, viz. $\Delta T/T = \Delta\rho/\rho = 2/3$ and the density gradient may be strong enough to generate important inviscid effects.

4.1 Mean quantities

Figure 6 shows that Case A is in good agreement with previous incompressible DNS (Kim *et al.*, 1987) for the mean velocity profile. The expected (for

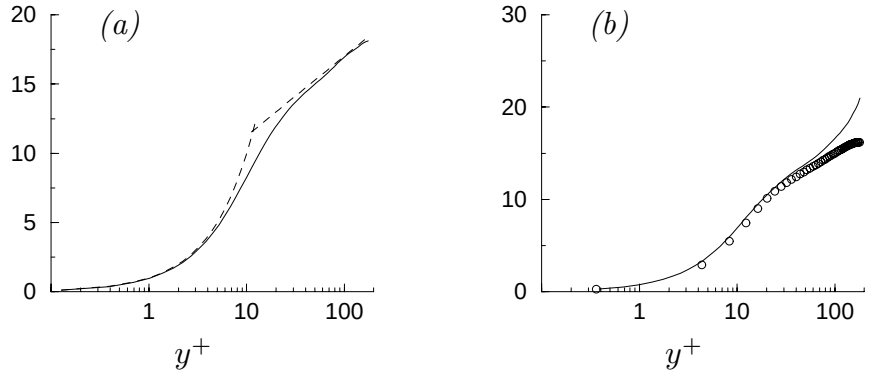

FIGURE 6. Mean profile of velocity (a) and temperature (b) for Case A. Wall units. - - - - : Law-of-the-wall; ∘ : Kader's formula ——— : Case A.

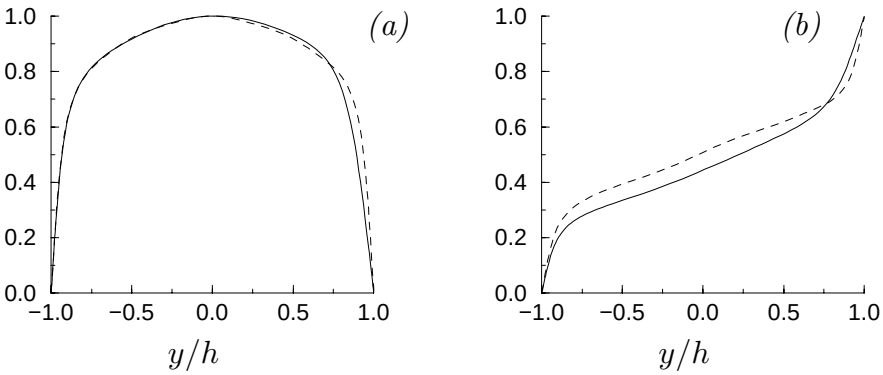

FIGURE 7. Mean profile of velocity (a) and temperature (b) in global coordinates. - - - - : Case A; ——— : Case B. Non-dimensionalization is u/u_{max} and $(T - T_1)/(T_2 - T_1)$.

the Reynolds number R_τ considered) law-of-the-wall $u^+ = 2.5ln(y^+) + 5.5$ is obtained, and there is good agreement with Kader's formula for the mean temperature. The non-dimensionalization is such that $T^+ = P_r y^+$ in the limit $y^+ \to 0$, viz. $T^+ = (T_w - T)/(B_q T_w)$ or $T^+ = (T_w - T)\rho_w C_p u_\tau / q_w$. Note that the linear behavior for T near $y^+ = 180$ is related to the inflexion point near the centerline, as shown in Fig. 7. This figure also shows the profiles for Case B. The temperature difference is strong enough to induce a significant asymmetry in the mean quantities. The temperature gradient is smaller near the hot wall so that, with the Sutherland's law Eq. (38), the heat flux is the same in absolute value at both sides. In semi-log plot, the mean velocity profile does not match the classical law-of-the-wall if scaled by the friction velocity. However, once transformed as proposed by Van Driest (1951), a logarithmic behavior is clearly obtained for the two sides of the channel. The slope remains close to its incompressible value whereas the additive constant is (slightly) greater for both the heated and the cooled wall. This puzzling result (there is no physical reason to believe that $C(B_q)$ is even) may be due to a low Reynolds number effect near the hot wall where density is lower and dynamic viscosity is higher. The temperature profiles (see Fig. 9) for Case A and Case B collapse only through

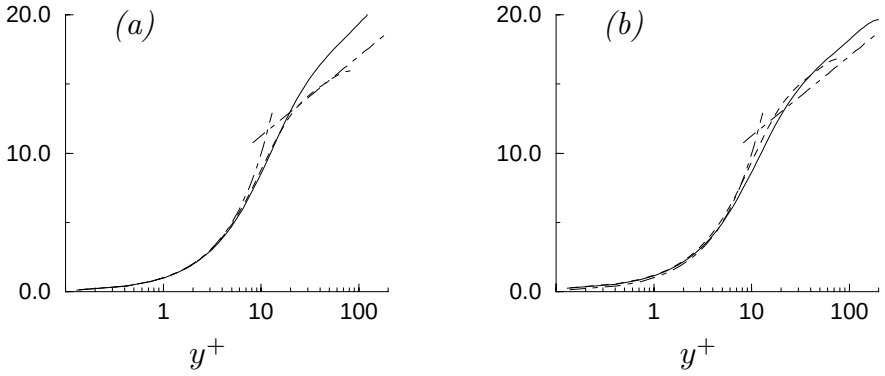

FIGURE 8. Mean profile of velocity in wall units for Case B. (a): non-transformed; (b): Transformed (Van Driest, 1951). ····· : $u^+ = y^+$ and $u^+ = 2.5ln(y^+) + 5.5$; ——— : Case B - Cold wall; - - - - : Case B - Hot wall.

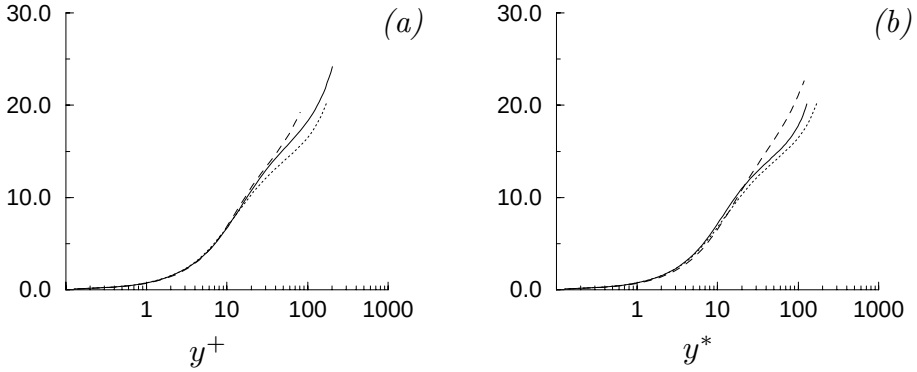

FIGURE 9. Mean profile of temperature in wall units. (a): classic scaling; (b): semi-local scaling. ····· : Case A; ——— : Case B - Cold wall; - - - - : Case B - Hot wall.

the beginning of the buffer layer ($y^+ \approx 15$). The Peclet number is so low near the hot wall ($P_e \approx 62$) that the linear behavior due to the inflexion point begins before the logarithmic region ($y^+ \approx 50$). A better collapse between Case A and the cold side of Case B is obtained when a semi-local scaling is used as suggested in Huang *et al.* (1995) (replacing ρ_w with $\rho(y)$, μ_w with $\mu(y)$ and $u_\tau = \sqrt{\tau_w/\rho_w}$ with $u_\tau^*(y) = \sqrt{\tau_w/\rho(y)}$ and then defining T^* and y^* in a similar manner as T^+ and y^+).

From Eq. (7), the mean normal velocity:

$$\overline{v} = \frac{1}{P_o R_e P_r}\left(\overline{k\frac{\partial T}{\partial y}} - \left|\overline{k\frac{\partial T}{\partial y}}\right|_w\right) \tag{42}$$

is not zero although the continuity equation requires that the Favre-averaged normal velocity $\widetilde{v} = \overline{\rho v}/\overline{\rho}$ is zero. However, the negative mean velocity generated by the turbulent heat transfer is only a small fraction ($\approx 1\%$) of the mean friction velocity $\overline{u_\tau}$. From Eq. (42), the total heat flux $q = -\overline{\rho}\widetilde{v''T''} + \overline{k\frac{\partial T}{\partial y}}$ is constant through the channel. Table II gives the principal mean physical characteristics for Case B.

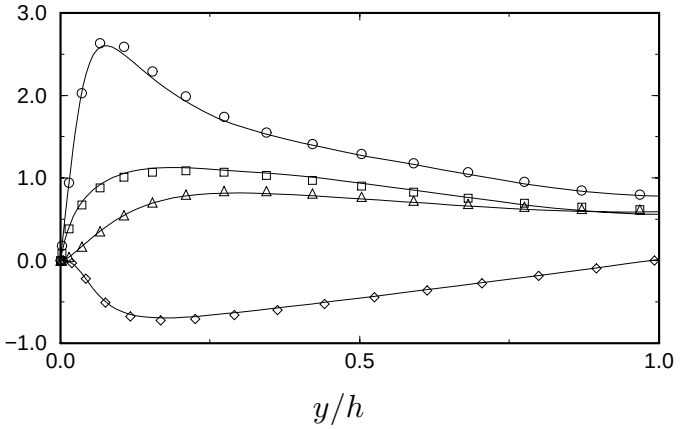

FIGURE 10. Velocity fluctuations for Case A. Wall units. Symbols from Kim *et al.* (1987). ○ : $u^+_{\rm rms}$, △ : $v^+_{\rm rms}$, □ : $w^+_{\rm rms}$, ◇ : $\overline{u'v'}^+$; ——— : Case A.

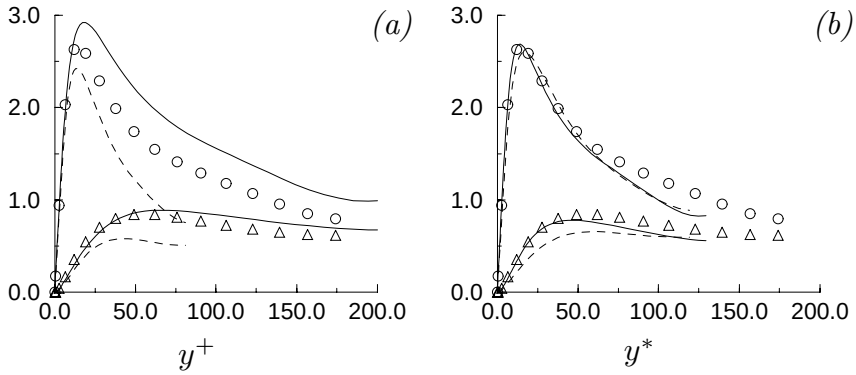

FIGURE 11. Velocity fluctuations in streamwise and normal direction. (a): classic scaling; (b): semi-local scaling. See previous figure for symbols. ——— : Case B - Cold wall; - - - - : Case B - Hot wall.

T_2/T_1	$u_{\tau 1}/\overline{u_\tau}$	$u_{\tau 2}/\overline{u_\tau}$	C_{f1}	C_{f2}	B_{q1}	B_{q2}
2	0.87	1.13	2.82×10^{-3}	2.48×10^{-3}	-0.018	0.014

Table II: Physical parameters for Case B.

The friction coefficient is based on the mean density in the channel and the maximum velocity. Due to density and dynamic viscosity variation, the friction velocity is higher at the hot wall but the shear stress is higher at the cold wall. The values obtained for the heat flux parameter B_q are small in absolute value compared to those in the DNS's of Coleman *et al.*, 1995 ($B_q = -0.05$ and -0.14) although the mean channel centerline-to-wall temperature ratios are equivalent (1.5 for Case B, compared to 1.4 and 2.5 for the compressible case). This is because the dissipation term in the internal energy equation is neglected in the low Mach approximation.

4.2 Turbulent fluctuations

For Case A, Fig. 10 shows a good agreement with previous incompressible DNS (Kim *et al.*, 1987) for the three velocity fluctuations and the Reynolds shear stress.

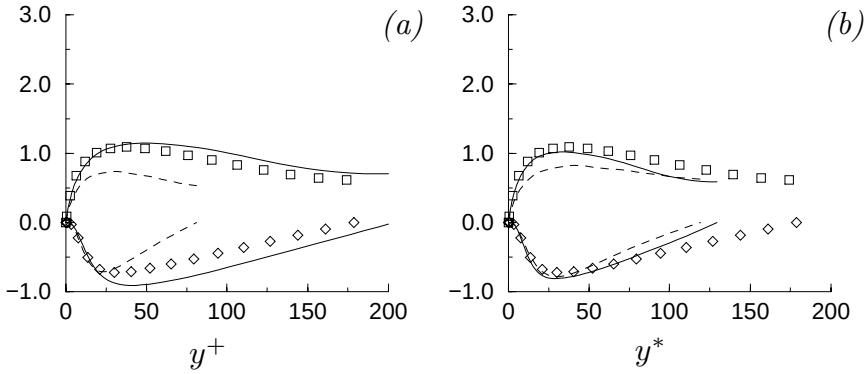

FIGURE 12. Velocity fluctuations in spanwise direction and correlation $\overline{u'v'}$. (a): classic scaling; (b): semi-local scaling. See previous figure for symbols. ——— : Case B - Cold wall; – – – – : Case B - Hot wall.

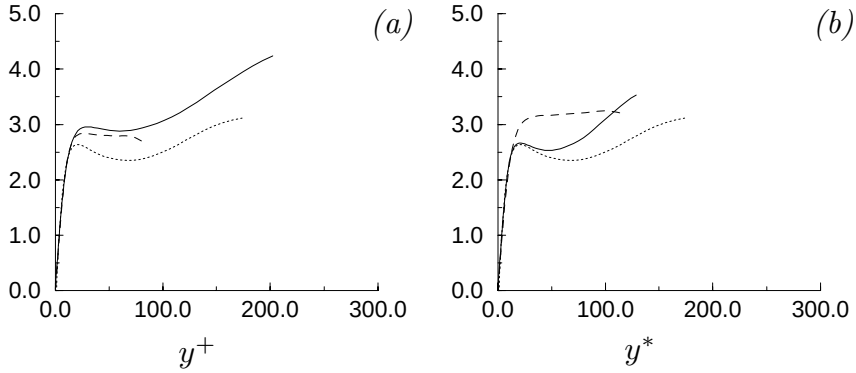

FIGURE 13. Temperature fluctuations. (a): classic scaling; (b): semi-local scaling. ····· : Case A; ——— : Case B - Cold wall; – – – – : Case B - Hot wall.

In Case B, these profiles are no longer symmetric and the inner layer appears to be thicker near the hot wall. Large departure from the incompressible case exists if the classic wall scaling is used (see Figs. 11a and 12a). The semi-local scaling allows the profiles to collapse very well. Still, the maximum of $v^*_{\rm rms}$ and $w^*_{\rm rms}$ is smaller in the hot side of Case B. The same trend was observed by Dailey & Pletcher (1998) in their strong heating case (in the supersonic channel flow studied by Coleman *et al.* (1995), both sides correspond to a strong cooling). It suggests that all the differences between the isothermal and heated flow cannot be reduced to a simple mean density effect. It is worth studying this point in more detail. The temperature fluctuations collapse neither for the classic nor for the semi-local scaling (see Fig. 13), except close to the wall and if only Case A and the cooled side of Case B are considered.

Gaviglio (1987) invokes a distinction between large and small scales in turbulence and argues that temperature and velocity fluctuations are highly correlated within large coherent structures. Defining the characteristic length as $l_u = \frac{u_{\rm rms}}{|\partial\overline{u}/\partial y|}$ and

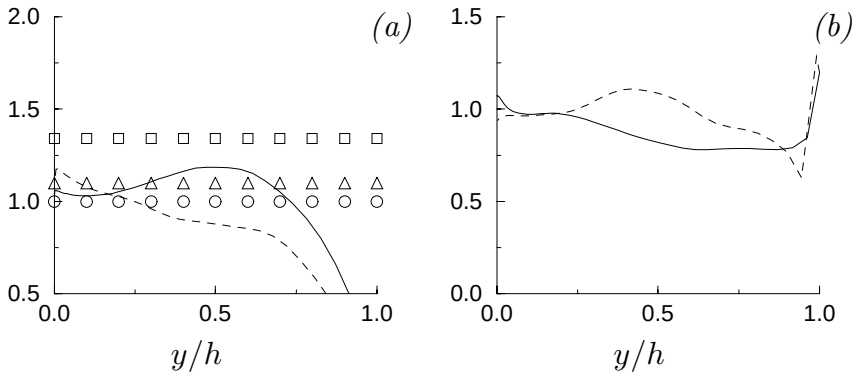

FIGURE 14. (a): $\frac{T_{\rm rms}}{u_{\rm rms}}\frac{|\partial\overline{u}/\partial y|}{|\partial\overline{T}/\partial y|}$ from the DNS Case B. ——— : cold wall; - - - - : hot wall; symbols: theoretical ratio from. ○ : Gaviglio (1987), △ : Huang *et al.* (1995), □ :Rubesin (1990). (b): Turbulent Prandtl number. ····· : Case A; ——— : Case B - Cold wall; - - - - : Case B - Hot wall.

$l_T = \frac{T_{\rm rms}}{|\partial\overline{T}/\partial y|}$ and assuming $l_u \propto l_T$, he derives:

$$\frac{T_{\rm rms}}{u_{\rm rms}}\frac{|\partial\overline{u}/\partial y|}{|\partial\overline{T}/\partial y|} = R_0 \tag{43}$$

Gaviglio's formulation imposes $R_0 = 1$ whereas Huang *et al.* (1995) propose $R_0 = 1/Pr_t$ ($Pr_t \approx 0.9$) and Rubesin (1990) chooses $R_0 = 1.34$. These analogies are tested in Fig. 14a and appear to give a reasonable representation of the present results. Figure 14a suggests that $R_0 = 1/Pr_t$ is a good choice. The turbulent Prandtl number is given in Fig. 14b. The cold side of the channel looks like the incompressible Case A with a peak around 1.1 at the wall, a plateau around $y^* \approx 40$, and a constant decrease through the center of the channel where $Pr_t \approx 0.7$. However, at the hot side of the channel, the turbulent Prandtl number is closer to a constant value and $Pr_t \approx 1$ would be a good approximation everywhere. It is not clear yet whether this different behavior is due to differing thermal conditions between the two walls, or whether it simply reflects a low-Reynolds number effect ($R_{\tau 2}$ is half $R_{\tau 1}$). The same question arises in looking at the correlation coefficients for the shear stress and the heat fluxes (Fig. 15). The main differences appear in the hot side of the channel where the Reynolds number is small. The maximum of R_{uv} and R_{vT} is located further from the wall in Case B, but the difference disappears when wall units are adopted. However, the profile of R_{uT} is fuller in the heated case with a larger negative correlation between u and T ($R_{uT} \approx -0.80$ compared to $R_{uT} \approx -0.60$ at $y/h = 0.5$). A scaling argument can hardly explain the difference. Kim & Moin (1987) did not observe that $|R_{uT}|$ increases for lower Peclet numbers.

4.3 Higher-order statistics

The computed skewness and flatness factors for u and v are shown in Figs. 16 and 17. The adequacy of the sample size used to compute the higher-order statistics is only marginal for Case B. However, these quantities are strongly related to the

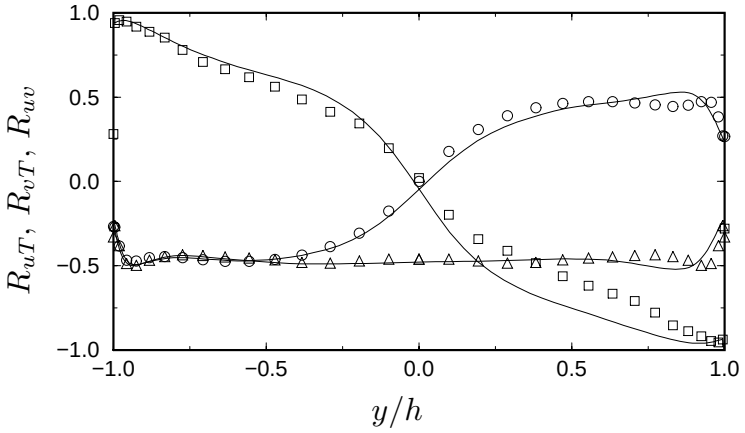

FIGURE 15. Correlation coefficients for Case B. Symbols from Kim *et al.* (1987). ○ : R_{uv}, △ : R_{vT}, □ : R_{uT}; ——— : Case B.

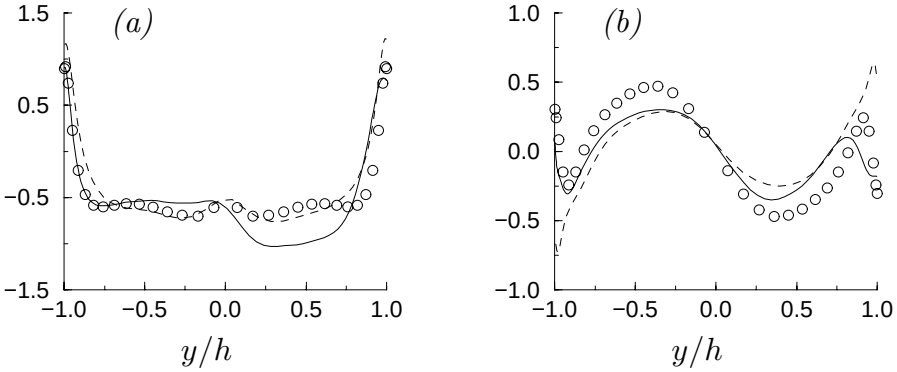

FIGURE 16. Skewness factors of u (a) and v (b). ——— : Case B; - - - - : Incompressible DNS, $R_\tau = 110$; ○ : Incompressible, $R_\tau = 180$, from Kim *et al.*

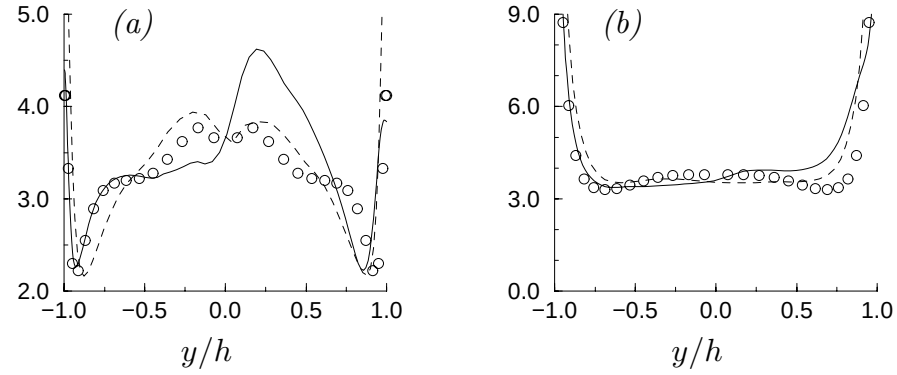

FIGURE 17. Flatness factors of u (a) and v (b). ——— : Case B; - - - - : Incompressible DNS, $R_\tau = 110$; ○ : Incompressible, $R_\tau = 180$, from Kim *et al.*

turbulence structure, and it is worth considering how they are modified by a strong heating/cooling. In Figs. 16 and 17, the results for Case B are compared to the incompressible data of Kim *et al.* (1987). To distinguish between the heat transfer

and the Reynolds number effect, a DNS of an incompressible channel flow at very low Reynolds number ($R_\tau = 110$) was performed with the fourth-order accurate code of Morinishi *et al.* (1998). The domain size for this simulation is ($4\pi h$,$2h$,$4\pi/3h$) and the grid contains 72x50x60 cells. Although $R_{\tau 2}$ is only about 80 in Case B, the incompressible simulation with $R_\tau = 110$ is adequately representative of the hot (upper) half of the channel in Case B. Indeed, because of the rapid near-wall variations of mean properties, the Reynolds number $R^*_{\tau 2}$ based on properties evaluated locally is equal to 110 in Case B at the distance $0.4h$ from the hot wall.

The skewness factor of the streamwise velocity u (see Fig. 16a) is roughly -0.5 to -0.6 for $y^+ \approx 50$ for the incompressible DNS's at $R_\tau = 180$ and $R_\tau = 110$. At the same time, the normal velocity (see Fig. 16b) is skewed positively in the lower half-channel and negatively in the upper one. It is known that these features of the skewness factors correspond to large excursions of fluid from the walls to the core region. Figure 16a shows that the skewness factor of u in the heated (upper) half-channel of Case B is approximately twice as large as in the incompressible cases. This strongly suggests that the density gradient enhances the ejection events in this region. The same trend is visible in Fig. 16b, which also suggests that the ejection events are weakened in the cooled (lower) half-plane. These findings would be consistent with the existence of a force that pushes the lumps of fluid from the hot to the cold wall. Wardana *et al.* (1992) supposed that the thermal expansion was responsible for the modifications observed in the turbulence structure. From Eq. (42), the mean dilatation in Case B produces negative mean momentum whose modulus is roughly $\rho|q_w|/P_o$. It acts on turbulent structures with time scale $\alpha h/u_\tau$, where $\alpha < 1$ expresses that the vortices are smaller than the channel half-height ($\alpha \approx 0.1$ at the distance $y = 0.2h$ from the wall). Requiring that the resulting impulsion, $\rho|q_w|u_\tau/(P_o \alpha h)$, is of the same order of magnitude as the viscous force, $\tau_w/h = \rho u_\tau^2/h$, one obtains the estimate $B_q \approx 0.1$ for the heat flux parameter. In Case B, as the modulus of B_q is of order 10^{-2}, it is unclear whether or not thermal expansion is significant. The inviscid force studied by Eames & Hunt (1997) offers an alternative to the mean thermal expansion to explain the modifications in the turbulence structure. It has the right sign (it is oriented from the hot wall to the cold wall) and the relative density variation $\Delta\rho/\rho$ is of order 1 in Case B, so that this force is not negligible (see the beginning of Section 4). Figures 17a and 17b show that the intermittency is higher in the heated side, smaller in the cooled side of the channel. This is consistent with the enhancement/damping of the strong bursting events illustrated above.

5. Discussion and future plans

The analogies developed in the context of supersonic boundary layers work well in the case of a low-speed flow with strong heat transfer. It is not very surprising since these analogies were derived assuming that compressibility effects are negligible except for the mean density gradient. An advantage of the present configuration is that each DNS provides information about both one positive and one negative heat flux parameter B_q. In this respect, the classical Van Driest transformation was tested for both a cooled and a heated wall, and the logarithmic behavior was well

retrieved for the mean velocity. The results suggest that the additive constant C is in both cases greater than its incompressible value. This unexpected result may be due to a low Reynolds number effect. Indeed, the Reynolds number R_τ at the hot wall is half its value at the hot wall and it is known that the additive constant in the law-of-the-wall increases for low Reynolds numbers. Assuming that the Reynolds number ratio $R_\tau^{hot}/R_\tau^{cold}$ behaves roughly like the temperature ratio T_1/T_2, it is clear that a DNS with strong heat transfer and sufficiently high Reynolds number everywhere in the domain would be very expensive. To this end, a 'non-physical' simulation where both the thermal conductivity and dynamic viscosity are inversely proportional to the temperature may serve as a less expensive way to minimize Reynolds number effects. Some differences appeared between the incompressible case and the cooled/heated channel that a re-scaling based on the mean density gradient was unable to eliminate altogether (amplitude of the peak in $v_{\rm rms}$ and $w_{\rm rms}$, shape of the profile of Pr_t, value of R_{uT}). The higher-order statistics reveal large modifications in the turbulence structure when the density gradient is not negligible. It is suggested that these modifications are related to a purely inviscid effect which pushes the turbulent structures towards the denser fluid. A case with a larger temperature ratio would be worth considering to investigate these differences in further detail.

P. Bradshaw and C. Pierce are acknowledged for their helpful comments on an earlier version of this manuscript.

REFERENCES

Bell, J. B. & Marcus, D. L. 1992 A second-order projection method for variable-density flows. *J. Comp. Phys.* **101,** 334-348.

Bradshaw, P. 1977 Compressible turbulent shear layers. *Ann. Rev. Fluid Mech.* **9,** 33-54.

Buell, J. C. 1990 Direct simulations of compressible wall-bounded turbulence. *CTR Annual Research Briefs.* Center for Turbulence Research, NASA Ames/ Stanford Univ., 347-356.

Cheng, R. K. & Ng, T. T. 1982 Some aspects of strongly heated turbulent boundary layers flows. *Phys. Fluids.* **25,** 8, 1333-1341.

Coleman, G. N., Kim, J., & Moser, R. D. 1995 A numerical study of turbulent supersonic isothermal-wall channel flow. *J. Fluid Mech.* **305,** 159-183.

Cook, A. & Riley, J. 1996 Direct numerical simulation of a turbulent reactive plume on a parallel computer. *J. Comp. Phys.* **129,** 263-283.

Dailey, L. D. & Pletcher, R. H. 1998 Large eddy simulation of constant heat flux turbulent channel flow with property variations. *AIAA 98-0791*

Eames, I. & Hunt, J. C. R. 1997 Inviscid flow around bodies moving in weak density gradients without buoyancy effects. *J. Fluid Mech.* **353,** 331-355.

Fernholz, H. H. & Finley, P. J. 1980 A critical commentary on mean flow data for two-dimensional compressible turbulent boundary layers. *AGARD-AG-253.*

Gaviglio, J. 1987 Reynolds analogies and experimental study of heat transfer in the supersonic boundary layer. *Int. J. Heat Mass Transfer.* **30,** 5, 911-926.

Huang, P. G. & Coleman G. N. 1994 Van Driest transformation and compressible wall-bounded flows. *AIAA J.* **32,** 10, 2110-2113.

Huang, P. G., Coleman, G. N. & Bradshaw, P. 1995 Compressible turbulent channel flows: DNS results and modeling. *J. Fluid Mech.* **305,** 185-218.

Kader, B. 1981 Temperature and concentration profiles in fully turbulent boundary layers. *Int. J. Heat Mass Transfer.* **24,** 9, 1541-1544.

Kasagi, N., Tomita, Y. & Kuroda, A. 1992 DNS of the passive scalar field in a turbulent channel flow. *ASME J. Heat Transfer.* **114,** 598-606.

Kim, J., Moin, P. & Moser, R. 1987 Turbulence statistics in fully developed channel flow at low Reynolds number. *J. Fluid Mech.* **177,** 133-166.

Kim, J. & Moin, P. 1987 Transport of passive scalars in a turbulent channel flow. *Turbulent Shear flows.* **6,** 85-96.

McMurthry, P., Jou, W., Riley, J. & Metcalfe, R. 1986 DNS's of a reacting mixing layer with chemical heat release. *AIAA J.* **24,** 6, 962-970.

Morinishi, Y., Lund, T., Vasilyev, O. & Moin, P. 1998 Fully Conservative higher order finite difference schemes for incompressible flow. *J. Comp. Phys.* **143,** 1, 90-124.

Morkovin, M. V. 1962 *Effects of compressibility on turbulent flows*, Coll. CNRS No. 108, Mécanique de la Turbulence, 367-380.

Paolucci, S. 1982 On the filtering of sound from the Navier-Stokes equations. *SAND82-8253,* Sandia National Laboratories, Livermore.

Rubesin, M.W. 1990 Extra compressibility terms for Favre-averaged two-equation models of inhomogeneous turbulent flows. *NASA CR-177556.*

Spalart, P. 1987 Hybrid RKW3 + Crank-Nicolson scheme. *Internal Report,* NASA-Ames Research Center, Moffett Field, CA.

Spina, E. F., Smits, A. J. & Robinson, S. K. 1994 The physics of supersonic turbulent boundary layers. *Ann. Rev. Fluid Mech.* **26,** 287-319.

Suslov, S. & Paolucci, S. 1995 Stability of mixed-convection flow in a tall vertical channel under non-Boussinesq conditions. *J. Fluid Mech.* **302,** 91-115.

Van Driest, E. R. 1951 Turbulent boundary layers in compressible fluids. *J. Aero. Sci.* **18,** 3, 145-160.

Wang, W. & Pletcher, R. 1996 On the large eddy simulation of a turbulent channel flow with significant heat transfer. *Phys. Fluids.* **8,** 12, 3354-3366.

Wardana, I. N. G., Ueda, T. & Mizomoto, M. 1992 Structure of turbulent two-dimensional channel flow with strongly heated wall. *Exp. Fluids.* **13,** 17-25.

Wardana, I. N. G., Ueda, T. & Mizomoto, M. 1994 Effect of strong wall heating on turbulence statistics of a channel flow. *Exp. Fluids.* **18,** 87-94.